Electric-field fluctuations in random dielectric composites

H. Cheng and S. Torquato

Department of Civil Engineering and Operations Research, and Princeton Materials Institute, Princeton University,
Princeton, New Jersey 08540

When a composite is subjected to a constant applied electric, thermal, or stress field, the associated local fields exhibit strong spatial fluctuations. In this paper, we evaluate the distribution of the local electric field (i.e., all moments of the field) for continuum (off-lattice) models of random dielectric composites. The local electric field in the composite is calculated by solving the governing partial differential equations using efficient and accurate integral equation techniques. We consider three different two-dimensional dispersions in which the inclusions are either (i) circular disks, (ii) squares, or (iii) needles. Our results show that in general the probability density function associated with the electric field for disks and squares exhibits a double-peak character. Therefore, the variance or second moment of the field is inadequate in characterizing the field fluctuations in the composite. Moreover, our results suggest that the variances for each phase are generally not equal to each other. In the case of a dilute concentration of needles, the probability density function is a singly peaked one, but the higher-order moments are appreciably larger for needles than for either disks or squares. [S0163-1829(97)03337-7]

I. INTRODUCTION

In the study of heterogeneous materials, much effort has been devoted to determining the effective transport and mechanical properties of the composite material.[1–5] The analysis and evaluation of the distribution of the local field (i.e., fluctuations of the local field) has received far less attention. Nonetheless, the distribution of the local field is of great fundamental and practical importance in understanding many crucial material properties such as the breakdown phenomenon[6,7] and the nonlinear behavior of composites.[8]

To show the importance of the local-field distribution, let us begin with the effective property itself. It is well known that in a statistically homogeneous and isotropic dielectric composite, the effective dielectric constant ϵ_{eff} of the composite can be defined through the following two equivalent relations:

$$\langle \mathbf{D}(\mathbf{r}) \rangle = \epsilon_{eff} \langle \mathbf{E}(\mathbf{r}) \rangle, \tag{1}$$

$$\langle \epsilon(\mathbf{r}) \mathbf{E}(\mathbf{r})^2 \rangle = \epsilon_{eff} \langle \mathbf{E}(\mathbf{r}) \rangle^2, \tag{2}$$

in which $\mathbf{E}(\mathbf{r})$ is the local electric field at position $\mathbf{r}$ in the composite, $\mathbf{D}(\mathbf{r}) = \epsilon(\mathbf{r}) \mathbf{E}(\mathbf{r})$ is the displacement field, $\epsilon(\mathbf{r})$ is the local dielectric constant, and angular brackets $\langle \rangle$ denote the averaging for an ergodic system, either an ensemble or a volume average. We see here that the effective dielectric constant is determined from lower moments of the local field.

The local-field distribution is also fundamental to understanding material failure or breakdown phenomenon. Breakdown phenomena have received considerable attention in recent years (see Refs. 9–14 and references therein). Dielectric (elastic) breakdown in a composite material occurs at localities where the field is the highest[6] or at "hot spots" where the local Joule heat [defined as $\epsilon(\mathbf{r}) \mathbf{E}(\mathbf{r})^2$] is very large.[7]

Thus breakdown in the composite is generally related to $\max(|\mathbf{E}(\mathbf{r})|)$, which can be expressed as

$$\max(|\mathbf{E}(\mathbf{r})|) = \lim_{k \to \infty} \langle \mathbf{E}(\mathbf{r})^{2k} \rangle^{1/2k}, \tag{3}$$

where $\langle \mathbf{E}(\mathbf{r})^{2k} \rangle$ is the even-order moment of the field.

The effective cubic nonlinearity coefficient[8] b_{eff} of the composite can be calculated by the relation

$$\langle b(\mathbf{r}) \mathbf{E}(\mathbf{r})^4 \rangle = b_{eff} \langle \mathbf{E}(\mathbf{r}) \rangle^4, \tag{4}$$

where $b(\mathbf{r})$ is the local nonlinear conductivity coefficient. Although b_{eff} is a nonlinear property of the composites, it was shown that it can be approximated, to the first order of the nonlinearity, by linear composites with the same microstructure through Eq. (4). From this nonlinear conductivity, one can further obtain the resistance fluctuation noise of the composites known as "flicker" noise. The flicker noise is defined as

$$\frac{1}{V} \frac{b_{eff}}{\epsilon_{eff}^2},$$

where ϵ_{eff} is the effective dielectric constant.

Previous work on field (or voltage) distribution in composites on lattice models can be found in the papers by de Arcangelis et al.,[15] Sheng and Chen,[16] and Helsing et al.[7] Sheng and Chen found that the local-field distribution generally exhibits a double-peak character in their models (the origin of which is different than what we find for continuum models). For continuum models, Beran[17] and Axell[18] derived bounds for the variance of the fields within each phase, while Bobeth and Diener[19] obtained approximate expressions for the same quantity. The results of Bobeth and Diener and Axell were established upon a result which states that the

effective dielectric constant of the composite is related to the ensemble average of the second moment of the field in each phase according to

$$\frac{\partial \epsilon_{\text{eff}}}{\partial \epsilon_i} = \frac{\langle \chi^{(i)}(\mathbf{r}) \mathbf{E}(\mathbf{r})^2 \rangle}{\langle \mathbf{E}(\mathbf{r})^2 \rangle}, \tag{5}$$

where $\chi^{(i)}(\mathbf{r})$ denotes the characteristic function of phase i. This relation was derived by Bergman[20] as a consequence of an analytical property of ϵ_{eff} as a function of ϵ_i. Among other results, we will show that the variance or second moment of the field is inadequate in describing the field fluctuations.

As we have pointed out, the most comprehensive numerical work on field distributions has been carried out for lattice models. A primary intent of the present work is to accomplish this task for continuum models of composites. Our model two-dimensional composite materials are made by embedding inclusions of one material into a uniform matrix of another material. We consider three different types of inclusions: (i) disks, (ii) squares, and (iii) needles. In each case, the applied electric field $\mathbf{E}_0$ [equal to the average field $\langle \mathbf{E}(\mathbf{r}) \rangle$] is directed along the x direction and we determine the probability density function $f(E_x(\mathbf{r})/E_0)$, where $E_x(\mathbf{r})$ is the x component of the local field $\mathbf{E}(\mathbf{r})$ and $E_0 = |\mathbf{E}_0|$. The quantity $f(E)dE$ is the probability that E has a value between E and $E + dE$. We will also calculate the kth moment $\langle |E_x(\mathbf{r})|^k \rangle$ of the field distribution. For reasons of mathematical analogy, our results for the local field translate immediately into equivalent results for the local electric field, local temperature gradient, and local magnetic field in the problems of electrostatics, steady-state heat conduction, and magnetostatics, respectively.

The remainder of this paper is organized as follows: In Sec. II, we will describe briefly the formulation of the problem and the numerical method that we will use to solve for the field. In Sec. III, we present our calculations on the distributions of the field for the three types of composites that we described earlier. Section IV contains some concluding remarks.

II. FORMULATION AND NUMERICAL TECHNIQUES

In order to show how the local field is distributed in a composite, one needs to solve the field accurately. To obtain the field, we must solve the governing Maxwell equation directly. The basic method to solve the Maxwell equation was devised first by Rayleigh[21] about a century ago, in an effort to improve the approximation formula given even earlier by Lorentz and Lorenz for the effective conductivity. Considerable progress has been made to improve this method in the past few decades. Recently, this method has been extended successfully by Greengard and Moura[22] to treat problems with complex geometries and with near singular interactions between inclusions.[23] However, most of this effort was directed towards finding the effective properties after solving the Maxwell equations. The analysis of the local field itself remains to be addressed using these accurate numerical techniques.

The numerical calculation of the field distribution consists of three steps. In the first step, we solve an integral equation

derived from the time-independent Maxwell equations employing the method developed by Greengard and Moura.[22] In the second step, we compute the electric field from the surface charge density obtained after solving the integral equation. This amounts to performing a numerical integration of the single layer potential, as defined below in Eq. (15). Unlike the calculation of the effective conductivity, which can be obtained from the charge density easily and accurately by a simple application of Green's formula, the evaluation of the field presents a much greater challenge numerically, since the kernel of the single layer potential is nearly singular if the target point (at which we want to compute the field) coincides or lies very close to one of the source points. The accurate evaluation of the integrals in such cases is extremely important for the accurate determination of the fields, because the contribution from the near source points to the field of a target point is likely to have the same magnitude as that from distant source points. In such cases, we greatly refine the local discretization to ensure the accuracy of the field, using the fact that the kernel is nonoscillating despite its integrable near singularity.[24] In the final step of the calculation, we perform statistical analyses on the sampling data of the field obtained for each model composite in order to determine the probability density function f as well as the moments of the field.

A. Formulation

Consider a two-phase random composite consisting of a matrix phase 1 region V_1 possessing a dielectric constant ϵ_1 and an inclusion phase 2 region V_2 possessing a dielectric constant ϵ_2. The standard time-independent Maxwell equations governing the electric field $\mathbf{E}(\mathbf{r})$ and displacement field $\mathbf{D}(\mathbf{r})$ in phase i of a dielectric composite are

$$\nabla \cdot \mathbf{D}(\mathbf{r}) = 0, \tag{6}$$

$$\nabla \times \mathbf{E}(\mathbf{r}) = 0, \tag{7}$$

$$\mathbf{D}(\mathbf{r}) = \epsilon(\mathbf{r}) \mathbf{E}(\mathbf{r}). \tag{8}$$

Here

$$\epsilon(\mathbf{r}) = \epsilon_1 \chi^{(1)}(\mathbf{r}) + \epsilon_2 \chi^{(2)}(\mathbf{r}) \tag{9}$$

is the local dielectric constant where

$$\chi^{(i)}(\mathbf{r}) = \begin{cases} 1, & \mathbf{r} \in V_i, \\ 0, & \text{otherwise,} \end{cases}$$

is the characteristic function of phase i.

It is convenient to study this problem via the electric field potential defined as

$$\mathbf{E}(\mathbf{r}) = -\nabla u(\mathbf{r}). \tag{10}$$

The scalar potential $u(\mathbf{r})$ is the solution of the following boundary value problem:

$$\nabla \cdot (\epsilon(\mathbf{r}) \nabla u(\mathbf{r})) = 0, \quad \mathbf{r} \in V_i, \quad (i = 1, 2), \tag{11}$$

$$u_+(\mathbf{r}) = u_-(\mathbf{r}), \quad \mathbf{r} \in \partial V_2, \tag{12}$$

$$\epsilon_1 \frac{\partial u_+(\mathbf{r})}{\partial n} = \epsilon_2 \frac{\partial u_-(\mathbf{r})}{\partial n}, \quad \mathbf{r} \in \partial V_2, \qquad (13)$$

where u_+ and u_- are the potentials as one approaches the inclusion surface from the matrix and inclusion side, respectively, and $\partial/\partial n$ is the standard normal derivative taken on the inclusion surface with the normal vector pointing outward from the inclusion. Relations (11)–(13) do not in general define a well-posed boundary value problem and an extra boundary condition is needed to guarantee the well posedness.

Before giving this condition, we first describe our composite model in more detail. The two-dimensional random dielectric composites under consideration are built by first randomly distributing a collection of inclusion into a square region—the generic unit cell. This unit cell is replicated periodically in both x and y directions to model an infinite medium. For simplicity, let us assume the unit cell to be $[-0.5,0.5] \times [-0.5,0.5]$ and the external electric field $\mathbf{E}_0 = (E_{0x}, E_{0y})$. For such a unit cell we require

$$u(x+1,y) = u(x,y) - E_{0x},$$

$$u(x,y+1) = u(x,y) - E_{0y}, \qquad (14)$$

where $(x,y) = \mathbf{r}$ is the componentwise position vector. Relations (11)–(14) combine to define a well-posed partial differential equation system which is solved for $u(\mathbf{r})$. The electric field is then calculated through Eq. (10).

We look for the solution of Eqs. (11)–(14) in the form of a single-layer potential

$$u(\mathbf{r}) = u_0(\mathbf{r}) + \sum_i \int_{\partial V_i} G(\mathbf{r}, \widetilde{\mathbf{r}}_i) \rho_i(\widetilde{\mathbf{r}}_i) ds_{\widetilde{\mathbf{r}}}, \qquad (15)$$

in which $u_0(\mathbf{r}) = -\mathbf{r} \cdot \mathbf{E}_0$. The summation is summed over all inclusions in the entire space, ∂V_i is the boundary of the ith inclusion, and $G(\mathbf{r}, \widetilde{\mathbf{r}}) = (1/2\pi) \ln|\mathbf{r} - \widetilde{\mathbf{r}}|$ is the two-dimensional fundamental solution of the Laplace's equation. $\rho_i(\widetilde{\mathbf{r}}_i)$ is the unknown surface charge density defined on ∂V_i. From periodicity, it is clear that only those $\rho_i(\widetilde{\mathbf{r}}_i)$ defined for the inclusions inside the unit cell are independent. With the representation (15), one can deduce from Eqs. (11)–(14) the following system of Fredholm integral equations of the second kind for the unknown densities $\rho_i(\widetilde{\mathbf{r}})$:

$$2\beta \frac{\partial u_0(\mathbf{r}_i)}{\partial n_i} = \rho_i(\mathbf{r}_i) - 2\sum_j \beta \int_{\Gamma_j} \frac{\partial G(\mathbf{r}_i, \widetilde{\mathbf{r}}_j)}{\partial n_i} \rho_j(\widetilde{\mathbf{r}}_j) ds_{\widetilde{\mathbf{r}}}$$

$$\text{for } \mathbf{r}_i \in \partial V_i. \qquad (16)$$

Here j runs over all inclusions in the entire space and $\beta = (\epsilon_2 - \epsilon_1)/(\epsilon_2 + \epsilon_1)$ is the "polarizability" which depends on the phase contrast. We put the subscript i on the standard outward normal derivative to emphasize that it is taken at $\mathbf{r}_i$ on ∂V_i. The index i should range over all inclusions in the entire space, and hence there are infinitely many equations in Eq. (16). However, due to periodicity, only a finite number of them are necessary; i.e., we only need to run i over the inclusions in the unit cell.

B. Numerical techniques

To solve Eq. (16) numerically, the surface charge densities $\rho_i(\widetilde{\mathbf{r}})$ will be discretized on the boundary of the inclusions, and the integrals in Eq. (16) will be approximated by the piecewise trapezoidal rule. Hence, Eq. (16) becomes

$$2\beta \frac{\partial u_0(\mathbf{r}_i^l)}{\partial n_i} = \rho_i(\mathbf{r}_i^l) - \frac{1}{\pi} \sum_j \beta \sum_{k=1}^{N_j} \frac{\partial \ln|\mathbf{r}_i^l - \widetilde{\mathbf{r}}_j^k|}{\partial n_i} \rho_j(\widetilde{\mathbf{r}}_j^k) \delta s_j^k, \qquad (17)$$

where $l = 1,2,\ldots,N_i$, and N_i, N_j are the numbers of discretization points on the ith and jth inclusions, respectively, with i running over the inclusions in the unit cell and j covering the inclusions in the entire space. It is easy to see that the summation over j can be translated into a double sum—a lattice sum of a sum over all inclusions in the unit cell. At the removable singular point of the kernel of Eq. (17), i.e., $\mathbf{r}_i^l = \widetilde{\mathbf{r}}_j^k$, the exact limit $\frac{1}{2}\kappa(\mathbf{r}_i^l)$ is taken,[25] where $\kappa(\mathbf{r}_i^l)$ is the curvature of the boundary of the ith inclusion at $\mathbf{r}_i^l$.

The linear system (17) is solved iteratively using the generalized minimal residual method[26] (GMRES), and the fast multipole method[27] (FMM) is used to speed up the matrix-vector multiplication. An iterative method (GMRES) is favored because our linear system is generally very large and therefore a direct method is insufficient. In fact, had we not used the FMM, even the GMRES would be too time consuming to be performed on a workstation. The FMM is in general a fast and accurate method for calculating the Coulombic interactions among particles (see Ref. 26 and references therein). Here we used it to calculate the sum of the form

$$s_j = \sum_{i=1}^{K} q_i \ln|\mathbf{r}_i - \mathbf{r}_j|,$$

and its spatial gradient, which appeared in Eq. (17). We recall that

$$\frac{\partial \ln|\mathbf{r}_i^l - \widetilde{\mathbf{r}}_j^k|}{\partial n_i} = \mathbf{n}(\mathbf{r}_i^l) \cdot \nabla(\ln|\mathbf{r}_i^l - \widetilde{\mathbf{r}}_j^k|).$$

By using the FMM, we substantially reduced the amount of work of per matrix-vector production from $O(N^2)$ by a direct calculation to $O(N)$ in our case, where $N = \Sigma_j N_j$ is the dimension of the unknown vector. If there are no particularly strong interactions among the inclusions, the above method can resolve the boundary-value problem extremely well, and achieves spectral accuracy.[22]

Once the surface charge density has been solved successfully, the next stage in the calculation is to obtain the electric field at a collection of uniformly, but randomly, distributed points in the unit cell. Unlike the case of computing the effective conductivity from $\rho_i(\widetilde{\mathbf{r}}_i)$, the calculation of the field presents a much more difficult numerical task. The major obstacle is related to the evaluation of the integral in Eq. (15), which can be rewritten in terms of a target point $\mathbf{r}_t$ as

$$u(\mathbf{r}_t) = u_0(\mathbf{r}_t) + \sum_i \int_{\partial V_i} G(\mathbf{r}_t, \widetilde{\mathbf{r}}_i) \rho_i(\widetilde{\mathbf{r}}_i) ds_{\widetilde{\mathbf{r}}}.$$

Here we want to calculate the field at $\mathbf{r}_t$. However, in the case that $\mathbf{r}_t$ is very close or coincides with one of the discretization points $\widetilde{\mathbf{r}}_i$, the above integration becomes nearly singular because in the kernel we have $G(\mathbf{r}_t,\widetilde{\mathbf{r}}_i) = (1/2\pi)\ln|\mathbf{r}_t - \widetilde{\mathbf{r}}_i|$. To tackle this difficulty, we utilized the techniques described by Davis and Rabinowitz[24] for singular integration by greatly refining the local discretization intervals, together with an interpolation on the density whenever $|\mathbf{r}_t - \widetilde{\mathbf{r}}_i| < \varepsilon$, where ε is the preset tolerance. Another difficulty is related to the large scale calculations necessary at this stage of computation. Suppose we discretized the boundary of the inclusions in the unit cell by M points, and we want to obtain the field at N target points. A straightforward calculation of these N field values would require $O(M \times N)$ evaluations of the source to target influence. Fortunately, this difficulty can be overcome by another application of the fast multipole method. The FMM can reduce the work to an amount of $O(M+N)$ such evaluations.

For each model composite, with its inclusion type, inclusion volume fraction and dielectric constant ratio fixed, we calculated 200 000 sampling local-field values from many different realizations generated by the standard Metropolis Monte Carlo algorithm. From these sampling data, we first compute the probability density function $f(E_x(\mathbf{r})/E_0)$. In order to do so, we use a common binning procedure, for which we first divide the whole range of the field value into a number of ''bins (intervals),'' determine for each local-field value in the sample which bin it belongs, calculate the number of total field values in each bin, then the probability density f is approximated in the ith bin by the formula

$$f_i = \frac{T_i}{200\,000 \times N_{\mathrm{BW}}},$$

where T_i is the total number of occurrence in ith bin and N_{BW} is the bin width. The probability density function f will be shown in figures. Then we complete our statistical analysis by calculating some moments of the field distribution from the sampling data. The moments are presented in the form of

$$\langle |E_x(\mathbf{r})|^k \rangle^{1/k} / E_0, \qquad (18)$$

for $k = 1, 2, 3, 4, 5, 10, 15, 20, 25, 30, 35, 40, 45, 50$ and ∞. The case $k = \infty$ is simply the maximum value of the magnitude of the local field in the sample.

III. FIELD DISTRIBUTIONS

We examined the field distributions in three types of continuum composite materials under a uniform applied field. The composite materials are made by randomly distributing in a uniform background matrix phase either (i) circular disks, (ii) squares, or (iii) needle-shaped inclusions. The composites with disks are characterized by the uniform disk diameter d. For disks of diameter d at number density n, the volume fraction of the inclusions can be calculated by

$$\phi_2 = n\pi d^2/4. \qquad (19)$$

In the case of squares with a side length l, the inclusion volume fraction is

$$\phi_2 = 4nl^2. \qquad (20)$$

In the case of needles we actually use slender ellipses with an aspect ratio of 50. Letting the length of the long axis be denoted by b, the needle volume fraction is given by

$$\phi_2 = n\pi b^2/50. \qquad (21)$$

Before presenting our numerical results, it is useful to make some remarks. First, our general primary goal in this work is to give a basic analysis of the field distribution in the *entire* composite. Alternatively, one may look at the field distribution in *one phase* only, as suggested by Eq. (5). If one is interested only in breakdown phenomenon, it may be best to study the field distribution at the *phase interfaces* exclusively, because the potential and the components of the field are harmonic and thus achieve extreme values on the interfaces only. Second, our numerical method described in the previous section is capable of computing the local field at *any* position in the composite. However, for our continuum models, it is certainly impossible to obtain and analyze numerically the field at *all* points in the composite. Thus, a necessary approximation is to perform the analysis of the field distribution on a representative sample of the field. Our sample size is 200 000 field values for each specific composite, with its inclusion type, inclusion volume fraction, and dielectric constant ratio fixed. Such a sample is chosen from 20 realizations of the specified composite, each realization is solved separately and 10 000 field values are calculated from the solution. Last, all of our composite models are assumed to satisfy a *no-clustering condition*; i.e., the inclusions must lie at a minimum distance of one another. This minimum distance was set to be $0.005d$, $0.005\sqrt{2}l$, and $0.005b$ for disks, squares, and needles, respectively. This approximation is reasonable because it does not change the presence of the field distribution in a noticeable manner, and it can ease the computational effort dramatically. In all our calculations, the field is generated by a unit potential drop across the horizontal edges of the unit computational cell $[-0.5,0.5] \times [-0.5,0.5]$; i.e., we set $\mathbf{E}_0 = (1,0)$. This does not lead to a loss of generality because our composites are taken to be isotropic and homogeneous, and our results are normalized with respect to the applied field.

A. Disks

In this section, we will be concerned with the field distributions in composite materials made by embedding circular disks into a uniform matrix. The configurations were generated using standard Monte Carlo simulation techniques. We used 64 disks in all of our examples. A typical realization at the disk volume fraction of 0.4 is depicted in Fig. 1.

In Figs. 2–4 and Table I, we present our calculated field distributions for such composite materials for various volume fractions and dielectric constant ratios. In the figures, we plot the probability density function $f(E_x(\mathbf{r})/E_0)$ against $E_x(\mathbf{r})/E_0$. In the table, we give the calculated moments, defined by Eq. (18), from the sampling data as an approximation to that of the field distribution for each case. From Figs. 2–4, we see clearly that the probability density function of the field also exhibits a double-peak character. In general, the peak on the left side is determined by the field inside the
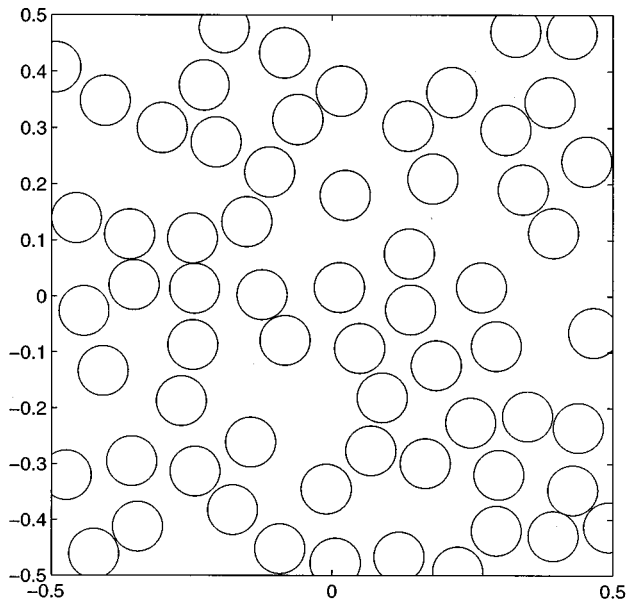
FIG. 1. A typical realization of randomly dispersed disk-shaped inclusions at an inclusion volume fraction $\phi_2 = 0.4$. The disk diameter is d. Note that the figure does not reflect the periodic boundary conditions used in the calculations.

phase with higher dielectric constant, and the peak on the right side is determined by the field inside the phase with lower dielectric constant.

To see the physical reason for this effect, let us assume that the inclusion phase has a higher dielectric constant than the matrix phase. The electric field inside the composite can be viewed as a perturbation of the imposed constant applied field. Without an inclusion phase, the perturbation effect is zero, and the electric field is just the applied field. The presence of higher dielectric constant inclusions induces polarization charges at the inclusion surfaces that weaken field inside the inclusion phase. In our case, this leads to a lower value of the x component of the electric field in the inclusion
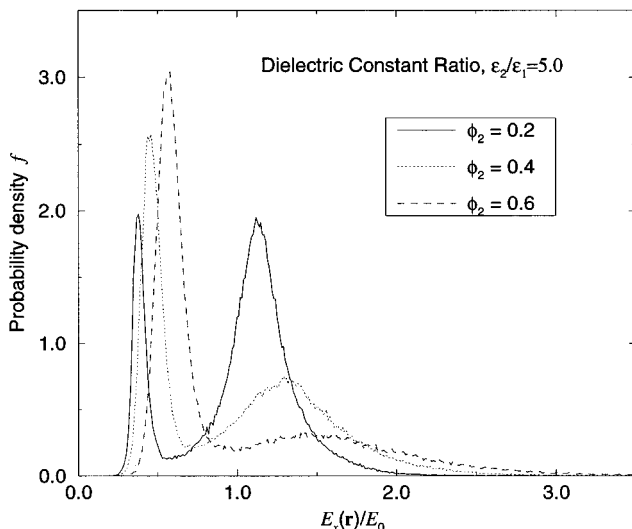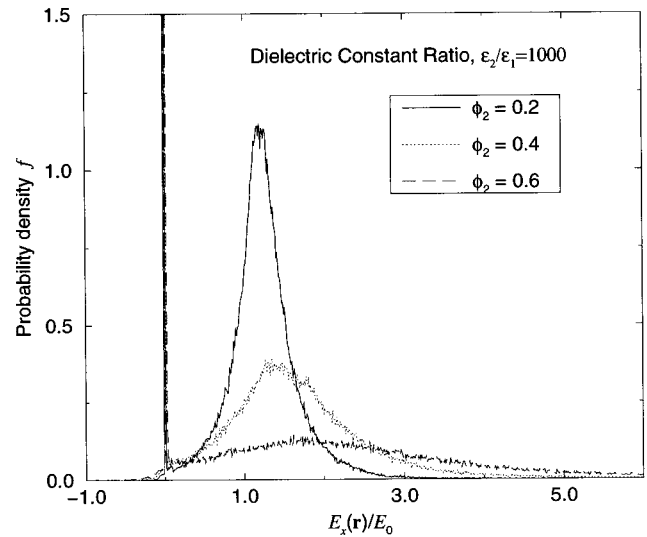

FIG. 2. The probability density function $f(E_x(\mathbf{r})/E_0)$ vs $E_x(\mathbf{r})/E_0$ for dispersions of randomly distributed disks in which the particle to matrix dielectric constant ratio $\epsilon_2/\epsilon_1 = 5.0$.

FIG. 3. The probability density function $f(E_x(\mathbf{r})/E_0)$ vs $E_x(\mathbf{r})/E_0$ for dispersions of randomly distributed disks in which the particle to matrix dielectric constant ratio $\epsilon_2/\epsilon_1 = 1000.0$.

phase. At the same time, the induced polarization charges enhance the field in the matrix phase, leading to a higher value of the x component of the electric field in the matrix phase than the applied field. Therefore, the left peak must lie to the left of the average field value and is associated with the field in the phase with a higher dielectric constant. Similarly, the right peak must lie to the right of the average field value and is associated with the field in the phase with a lower dielectric constant. This double-peak character indicates that the variance or second moment is generally not adequate in describing the field distribution in composites.

Double-peak behavior in the field distribution was also seen by Sheng and Chen[16] for a lattice model. However, the origin of the double-peak behavior observed in their study (due to two types of local environment) arises for different reasons. First, we consider all multipole contributions for a continuum dielectric model (random placement of inclusions of finite size in a matrix), whereas Sheng and Chen consider point dipole particles on a lattice. Second, they consider a modified electric field (the Lorentz field $\mathbf{E}_L$), as opposed to the Maxwell field that we compute. Third, in contrast to the pointwise field that we calculate throughout the entire composite, they determined the Lorentz field for each point particle. In order to make our field calculations equivalent to theirs, we would have to compute ''averaged'' Lorentz fields for each inclusion in the composite up to dipole contributions and randomly locate the particles on a lattice. We emphasize that the double-peak behavior that we find is due to high and low fields occurring in the low and high dielectric phases, respectively.

The first line of Table I shows not only that our calculation of the field is accurate, but also that the samples which we have taken to represent the field in the whole composite are quite adequate. The latter is true because our results here agree with the exact value for that line, which should be the applied field (1.000), to three figures.

In the disk-to-matrix dielectric constant ratio $\epsilon_2/\epsilon_1 = 5.0$ case (Fig. 2 and columns 2–4 of Table I), we see that the

TABLE I. The moments of the field distribution for composites with circular disks. Here k is the order of the moment, ϵ_2/ϵ_1 stands for the dielectric constant ratio, and ϕ_2 denotes the inclusion volume fraction. The data for $k=\infty$ are the observed maximum values of $|E_x|$. The last row gives the dimensionless effective dielectric constant of the composites.

| | $\epsilon_2/\epsilon_1=5.0$ | | | $\epsilon_2/\epsilon_1=1000.0$ | | | $\epsilon_2/\epsilon_1=0.001$ | | |
k	$\phi_2=0.2$	$\phi_2=0.4$	$\phi_2=0.6$	$\phi_2=0.2$	$\phi_2=0.4$	$\phi_2=0.6$	$\phi_2=0.2$	$\phi_2=0.4$	$\phi_2=0.6$
1	1.000	0.999	1.002	0.999	0.995	0.999	1.001	0.999	0.999
2	1.068	1.133	1.187	1.178	1.457	1.956	1.113	1.159	1.177
3	1.121	1.250	1.380	1.290	1.811	2.895	1.234	1.326	1.348
4	1.167	1.354	1.565	1.400	2.227	4.243	1.367	1.495	1.544
5	1.211	1.451	1.742	1.557	2.816	6.185	1.528	1.732	1.793
10	1.537	1.982	2.598	3.675	7.012	17.54	3.126	3.577	3.633
15	1.991	2.556	3.315	5.510	10.32	25.90	4.566	5.045	5.180
20	2.338	3.002	3.846	6.753	12.62	31.61	5.534	6.045	6.259
25	2.591	3.327	4.239	7.629	14.25	35.66	6.214	6.753	7.033
30	2.783	3.571	4.538	8.276	15.45	38.67	6.714	7.279	7.610
35	2.935	3.758	4.772	8.771	16.37	40.98	7.097	7.682	8.055
40	3.057	3.907	4.959	9.162	17.10	42.80	7.399	8.002	8.408
45	3.158	4.027	5.111	9.478	17.69	44.28	7.644	8.260	8.696
50	3.241	4.127	5.239	9.739	18.18	45.49	7.847	8.474	8.933
∞	4.132	5.187	6.609	12.43	23.21	58.07	9.984	10.72	11.40
$\epsilon_{\mathrm{eff}}/\epsilon_1$	1.316	1.767	2.417	1.532	2.592	4.979	0.649	0.388	0.199

field behaves nicely with its two peaks sharply separated and the first peak rises with the increasing of the disk (which is the phase with a higher dielectric constant) volume fraction, because of the increasing possibility of the sampling points being in the disks. In the case that the disks have a high dielectric constant ($\epsilon_2/\epsilon_1=1000.0$) (Fig. 3 and columns 5–7 of Table I), we see that while the field in the matrix phase (the second peak) behaves nearly the same as in previous case, the first peak now looks like a delta function at $E_x(\mathbf{r}) \approx 0$. In the case that the disks have a very low dielectric constant relative to the matrix ($\epsilon_2/\epsilon_1=0.001$), Fig. 4 and Table I show that the two peaks of the field distribution are not so well separated.

Beran[20] conjectured that in a two-phase composite material, the variance of the field in phase 1 is of the order of the variance of the field in phase 2, i.e.,

$$\widetilde{\sigma}_{E_1}^2 = O(\widetilde{\sigma}_{E_2}^2),$$
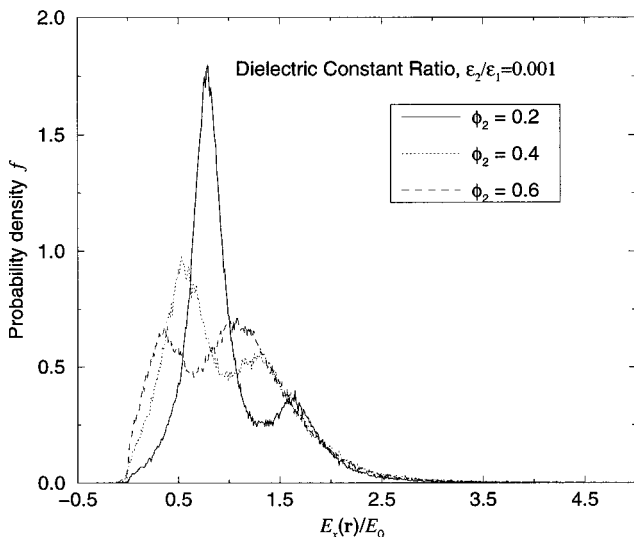
where

FIG. 4. The probability density function $f(E_x(\mathbf{r})/E_0)$ vs $E_x(\mathbf{r})/E_0$ for dispersions of randomly distributed disks in which the particle to matrix dielectric constant ration $\epsilon_2 A/\epsilon_1=0.001$.
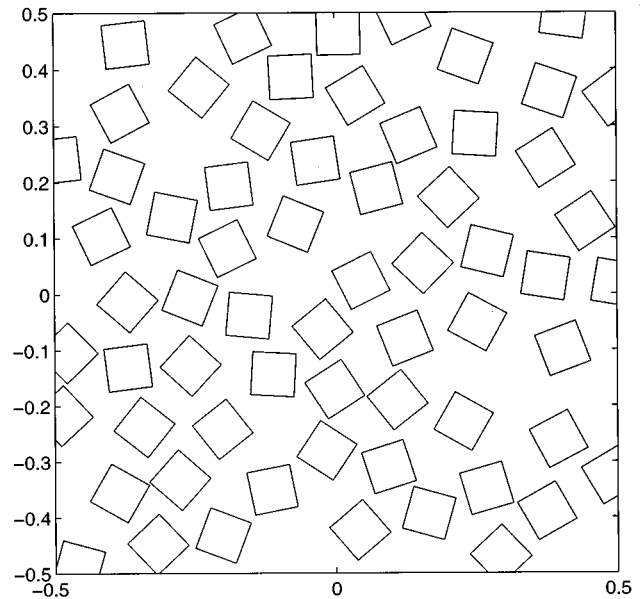

FIG. 5. A typical realization of randomly dispersed and randomly oriented square-shaped inclusions at an inclusion volume fraction $\phi_2=0.4$. The length of the square side is l. Note that the figures does not reflect the periodic boundary conditions used in the calculations.
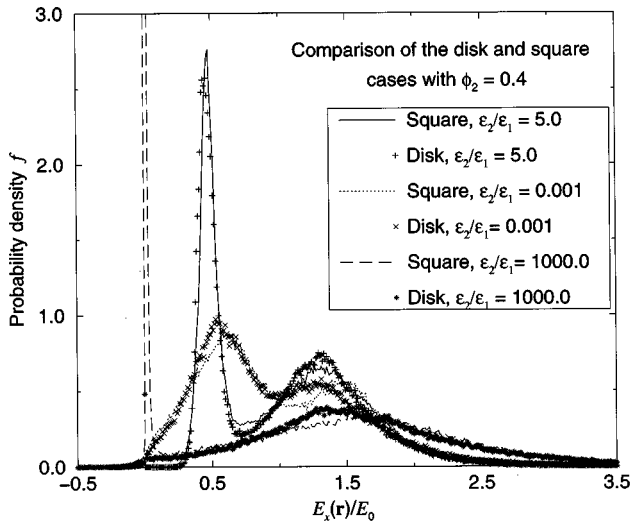
FIG. 6. The probability density function $f(E_x(\mathbf{r})/E_0)$ vs $E_x(\mathbf{r})/E_0$ for disperions of randomly distributed squares in comparison with that of the disk at volume fraction $\phi_2 = 0.4$, and dielectric constant ratio varied as $\epsilon_2/\epsilon_1 = 5.0$, 1000.0, and 0.001.

$$\tilde{\sigma}^2_{E_i} = \frac{\langle (\mathbf{E}_i - \langle \mathbf{E}_i \rangle) \cdot (\mathbf{E}_i - \langle \mathbf{E}_i \rangle) \rangle}{\langle \mathbf{E}_i \rangle \langle \mathbf{E}_i \rangle},$$

and $\mathbf{E}_i$ is the electric field in phase i. Beran assumed this relation to derive other results. While it is possible that this could be true for certain class of materials, we found no numerical evidence to support this conjecture for the models considered in the present work. This would certainly not be true for the highly conducting disk case for which the field in the inclusion phase is nearly uniform. Overall, the widths of

the two peaks [an indication of the variance of $E_x(\mathbf{r})/E_0$] were rather different from each other in our figures.

B. Squares

In this section, we calculate the field distribution in two dimensional dispersions in which the inclusions are squares. Of particular interest is how the presence of corners will affect the field distribution. The square-shaped inclusions in our model composites are randomly distributed and randomly oriented. A typical configuration at volume fraction 0.4 with 64 squares in the unit cell is depicted in Fig. 5. Our configurations for randomly distributed squares are generated by first generating a random distribution of disks with a desired volume fraction, and then making a square from each disk with a randomly chosen angle at which the first vertex of the square lies.

In Fig. 6 and columns 2–4 of Table II, we showed our calculated results of the field distribution in three cases of composite materials with randomly distributed square-shaped inclusions. The inclusion volume fraction is 0.4 for all examples. The dielectric constant ratios were varied as $\epsilon_2/\epsilon_1 = 5.0$, 1000.0, and 0.001. For comparison, we also included in Fig. 6 the results for the corresponding disk cases. From the figure, we see that field distributions for the case of squares nearly coincided with those for the disk case. One reason is probably that numerically we cannot calculate exactly the charge density at the corners because it is not well defined there, and thus we approximated the density by refining the discretization at the vicinity of corners but skipping the exact corner position, thereby limiting the true influence of the corners. This is exactly the reason that our observed maximum values from the sample are actually lower than that for disk case, for which the close interaction

TABLE II. The moments of the field distributions for the square- and needle-shaped inclusions. Here k is the order of the moment, ϵ_2/ϵ_1 stands for the dielectric constant ratio, and ϕ_2 denotes the inclusion volume fraction. The data for $k = \infty$ are the observed maximum values of $|E_x|$. The last line is the effective dielectric constant of the composites.

| k	Squares ($\phi_2 = 0.4$)			Needles ($\phi_2 = 0.012$)		
	$\epsilon_2/\epsilon_1 = 5.0$	$\epsilon_2/\epsilon_1 = 1000.0$	$\epsilon_2/\epsilon_1 = 0.001$	$\epsilon_2/\epsilon_1 = 5.0$	$\epsilon_2/\epsilon_1 = 100.0$	$\epsilon_2/\epsilon_1 = 0.001$
1	1.001	1.005	1.003	1.000	1.001	0.999
2	1.130	1.455	1.166	1.003	1.041	3.496
3	1.240	1.754	1.316	1.006	1.085	8.629
4	1.335	2.024	1.479	1.018	1.161	17.19
5	1.420	2.308	1.686	1.089	1.345	27.83
10	1.843	4.125	3.250	2.905	3.378	83.23
15	2.298	5.717	4.460	4.362	4.901	121.2
20	2.657	6.857	5.268	5.346	5.928	146.7
25	2.921	7.682	5.837	6.040	6.665	164.7
30	3.120	8.299	6.258	6.552	7.197	178.1
35	3.274	8.775	6.584	6.944	7.614	188.3
40	3.397	9.154	6.843	7.254	7.946	196.5
45	3.497	9.462	7.055	7.504	8.215	203.1
50	3.580	9.717	7.231	7.710	8.438	208.6
∞	4.470	12.39	9.162	9.842	10.77	265.9
$\epsilon_{\text{eff}}/\epsilon_1$	1.773	2.648	0.379	1.027	1.239	0.718
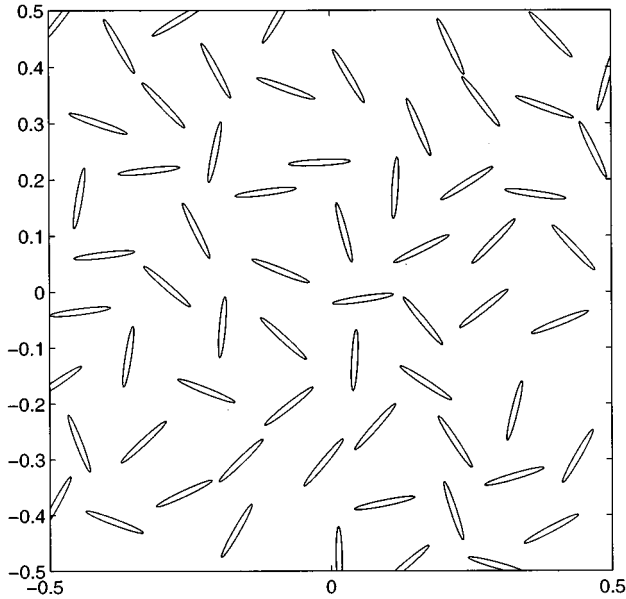
FIG. 7. A typical realization of randomly dispersed needle-shaped inclusions. The length of the needle is b. Aspect ratio here is 10. Our field distribution calculations are based on an aspect ratio of 50, however. Note that the figure does not reflect the periodic boundary conditions used in the calculations.

among inclusions is more likely due to our configuration generating process. A second reason is that even if we could calculate the density at the corners with more accuracy, it is still unlikely to change the field distribution in the whole composite vastly (this will certainly change the line of observed maximum value in the table, however). This is because the corners are rare and the chance of our sampling position (where we calculate the local field) lying very close to one of them is very small. While the corner effect is not strong enough to be seen on the local field distribution figure, we should also notice that the combined effect of the corners is certainly not negligible as far as the effective dielectric constant is concerned. Indeed, we do see a stronger influence on the effective dielectric constant due to the presence of the corners from the data in the table.

C. Needles

Here we present our calculations for random distributions of needles in a matrix for various phase dielectric constant ratios. In the case that the inclusions have a very small dielectric constant compared to that of the matrix phase, we mimic materials with cracklike flaws. Figure 7 displays a typical configuration of our composite material with 64 needle-shaped inclusions. The needles are randomly placed and randomly oriented. The generation of the configurations for randomly distributed needles is similar to that for squares. Specifically, we first generate a random distribution of disks of diameter d and then place a needle (of length d) with random orientation within each disk. As noted earlier, each needle is actually a very slender ellipse with an aspect ratio of 50.0. (In the figure, the aspect ratio is only 10.0.)

Our results on the field distributions for the case of needles are summarized in Fig. 8 and columns 5–7 of Table II. The needle volume fraction is merely 0.012 and three
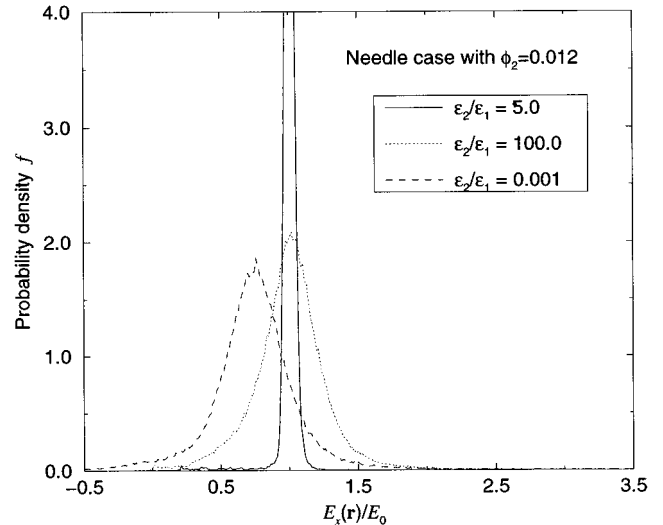

FIG. 8. The probability density function $f(E_x(\mathbf{r})/E_0)$ vs $E_x(\mathbf{r})/E_0$ for dispersions of randomly distributed needles with thee representative particle to matrix dielectric constant ratios.

different needle-matrix dielectric constant ratios were chosen: $\epsilon_2/\epsilon_1 = 5.0$, 100.0, and 0.001. The last case mimics the case of cracks. From Fig. 8, we see that the field distribution for needles becomes single peaked, especially for the case in which $\epsilon_2/\epsilon_1 = 5.0$, where it becomes δ-function-like with its top being cut off in the figure. The reason that the other peak disappears is simply because the needle phase volume fraction is sufficiently small such that the probability of sampling in the needle phase is very small. Notice that the peaks for $\epsilon_2/\epsilon_1 = 5.0$ (solid line) and $\epsilon_2/\epsilon_1 = 100.0$ (dotted line) lie to the right of $E_x(\mathbf{r})/E_0 = 1.0$. And the peak for the crack case $\epsilon_2/\epsilon_1 = 0.001$ (dashed line) lies to the left of $E_x(\mathbf{r})/E_0 = 1.0$. This is because in the first two cases, the inclusion phase has a higher dielectric constant, and in the last case, the dielectric constant of the needles is lower than that of the matrix, which confirms our earlier suggestions. Although we do not see strong field fluctuations from the plots of the probability density functions, a close examination of the moment data in Table II shows us that needles give rise to very high moment values, even though they occupy a small fraction of the space. Disks (or squares) at the same value of dielectric constant ratio ϵ_2/ϵ_1 require a much higher volume fraction to achieve similar values of the moments. We were able to capture the high-field behavior due to sharp ends in the needle case (unlike the instance of squares) for two reasons. First, the influence of the sharp ends of the needles is stronger than the influence of the corners of the squares. Second, we assume that each needle is actually a very slender ellipse whose boundary is smooth and is numerically more tractable.

IV. CONCLUSIONS

In this paper, we studied the local-field distributions for continuum (off-lattice) models of random dielectric composites. We considered three different two-dimensional dispersions in which the inclusions were either (i) circular disks, (ii) squares, or (iii) needles. The fluctuations were quantified in two ways: by computing the probability density function associated with the electric field and by computing the moments of the field. We showed that in general the probability

density function for disks and squares exhibits a double-peak character, similar to lattice models. Not surprisingly, therefore, the variance or second moment of the field is generally inadequate in characterizing the field fluctuations in the composite. In the case of a dilute concentration of needles, the probability density function is a singly-peaked one, but the higher-order moments are appreciably larger for needles than for either disks or squares.

[1] M. J. Beran, *Statistical Continuum Theories* (Wiley, New York, 1968).

[2] R. M. Christensen, *Mechanics of Composite Materials* (Wiley, New York, 1979).

[3] G. W. Milton and N. Phan-Thien, Proc. R. Soc. London, Ser. A **380**, 305 (1982).

[4] Z. Hashin, J. Appl. Mech. **50**, 481 (1983).

[5] S. Torquato, Appl. Mech. Rev. **44**, 37 (1991).

[6] Y. S. Li and P. M. Duxbury, Phys. Rev. B **40**, 4889 (1989).

[7] J. Helsing, J. Axell, and G. Grimvall, Phys. Rev. B **39**, 9231 (1989).

[8] O. Levy and D. J. Bergman, Phys. Rev. B **50**, 3652 (1994).

[9] M. Acharyya and B. K. Chakrabarti, Phys. Rev. E **53**, 140 (1996).

[10] D. Arnold, E. Cartier, and D. J. DiMaria, Phys. Rev. B **49**, 10 278 (1994).

[11] *Nonlinearity and Breakdown in Soft Condensed Matter*, edited by K. K. Bardhan, B. K. Chakrabarti, and A. Hansen, Lecture Notes in Physics, Vol. 437 (Springer-Verlag, Heidelberg, 1994).

[12] P. M. Duxbury, P. D. Beale, and P. L. Leath, Phys. Rev. Lett. **57**, 1052 (1986).

[13] P. M. Duxbury and P. L. Leath, Phys. Rev. Lett. **72**, 2805 (1994).

[14] M. Enokizono and H. Tsutsumi, IEEE Trans. Magn. **30**, 2936 (1994).

[15] L. de Arcangelis, S. Redner, and A. Coniglio, Phys. Rev. B **34**, 4656 (1986).

[16] P. Sheng and Z. Chen, Phys. Rev. Lett. **60**, 227 (1988).

[17] M. Beran, J. Math. Phys. (N.Y.) **21**, 2583 (1980).

[18] J. Axell, J. Appl. Phys. **72**, 1217 (1992).

[19] M. Bobeth and D. Diener, J. Mech. Phys. Solids **34**, 1 (1986).

[20] D. J. Bergman, Phys. Rep. **43**, 377 (1978).

[21] Lord Rayleigh, Philos. Mag. **34**, 481 (1892).

[22] L. Greengard and M. Moura, *Acta Numerica* (Cambridge University Press, Cambridge, England, 1994), p. 379.

[23] H. Cheng and L. Greengard, SIAM (Soc. Ind. Appl. Math.) J. Appl. Math. (to be published).

[24] P. J. Davis and P. Rabinowitz, *Methods of Numerical Integrations*, 2nd ed. (Academic Press, New York, 1986).

[25] G. B. Folland, *Introduction to Partial Differential Equations* (Princeton University Press, Princeton, NJ, 1976).

[26] Y. Saad and M. H. Schultz, SIAM (Soc. Ind. Appl. Math.) J. Sci. Stat. Comput. **7**, 856 (1986).

[27] L. Greengard, *The Rapid Evaluation of Potential Fields in Particle Systems* (MIT Press, Cambridge, MA, 1988).